

# Simplification of Corticosteroids Biosynthetic Pathway by Engineering P450BM3

Qihang Chen, Zikai Chao, Ke Wang, Xinglong Wang, Hao Meng, Xirong Liu, Xiaoyu Shan, and Jingwen Zhou\*



Cite This: ACS Catal. 2024, 14, 4117–4129



Read Online

ACCESS |

Metrics & More

Article Recommendations

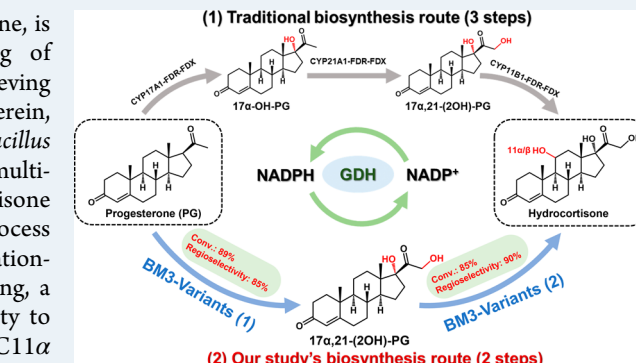
Supporting Information

**ABSTRACT:** Synthesis of corticosteroids, particularly hydrocortisone, is challenging owing to the complex network requiring pairing of cytochrome P450s with cytochrome P450 reductase (CPR) for achieving regionally selective hydroxylation modifications at multiple sites. Herein, we engineered a self-sufficient P450BM3 (CYP102A1 from *Bacillus megaterium*) for effectively reducing the traditionally complex, multi-enzyme cascade process (three steps and six enzymes) of hydrocortisone synthesis from progesterone (PG) to a simplified two-step process involving at least two enzymes. Driven by computational simulation-guided substrate access channel and heme center pocket engineering, a series of P450BM3 variants were gradually designed with the ability to catalyze C16 $\beta$ , C17 $\alpha$ , C21, and C17 $\alpha$ /21 oxidation of PG and C11 $\alpha$  oxidation of cortexolone (*c*). Subsequently, molecular dynamics simulations with an oxy-ferrous model of P450BM3 variants revealed that the glycine mutations of residues that are repulsive to the substrate allow for more stable exposure of the substrate above Fe=O. Finally, the developed P450 variants were employed to construct efficient *Escherichia coli* catalytic systems, which further achieved 11 $\alpha/\beta$ -hydrocortisone (f/e) production in one pot from 1 g/L PG at a molar conversion rate of 81 and 84% (912 and 955 mg/L), respectively. Thus, this study provides feasible strategies for simplifying the biosynthetic steps and biocatalysts for steroid pharmaceutical production.

**KEYWORDS:** steroid oxidation, corticosteroids, cytochrome P450, molecular dynamic simulation, enzyme engineering

## 1. INTRODUCTION

Steroids, composed of a complex cyclopentane-polyhydrophenanthrene structure, present anti-inflammatory and immunosuppressive effects and are used for treating various clinical diseases, including acute infections, inflammatory aftermath, autoimmune disorders of connective tissues, COVID-19, and acquired immunodeficiency syndrome (AIDS).<sup>1,2</sup> Introduction of the hydroxyl groups into the steroid backbone in a regioselective and stereoselective manner is an essential step for achieving ideal solubility as well as the physiological and pharmacological activity of steroids.<sup>3–6</sup> For instance, hydrocortisone, a typical corticosteroid with a progesterone (PG) skeleton and modified with three hydroxylations at C11 $\beta$ , C17 $\alpha$ , and C21, possesses potent anti-inflammatory and immunosuppressive properties, making it an ideal choice for treating conditions such as allergies, dermatitis, and adrenal dysfunction.<sup>7–9</sup> Nevertheless, given the abundance of inert C–H bonds in steroids, achieving precise single or multiple oxidations of the steroid backbone without generating excess byproducts remains a formidable task in synthetic chemistry.<sup>10,11</sup> Thus, targeting the oxidation of steroid backbones to synthesize high-value steroid pharmaceuticals in the process of producing hydroxyl-rich corticosteroids involves immense



challenges such as numerous reaction steps, generation of substantial undesired byproducts, and elevated synthesis costs.<sup>8,12</sup>

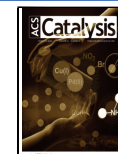
Cytochrome P450 enzymes (CYP450), a vast group of heme-binding proteins found across various organisms, play a crucial role in metabolizing a range of drugs and endogenous compounds owing to their ability to catalyze numerous oxidative transformations.<sup>13,14</sup> Several P450s have been identified and subsequently engineered for achieving precise oxidation of various carbon positions in the steroid backbone, such as androstanedione (AD), dehydroepiandrosterone, and testosterone.<sup>4,8,15</sup> In corticosteroids synthesis, the traditionally complex and multistep chemical synthesis of hydrocortisone has been streamlined by incorporating CYP11B1 for C11 $\beta$  hydroxylation and utilizing cortexolone (*c*) as the substrate, effectively circumventing the arduous 10–12-step purification

Received: December 18, 2023

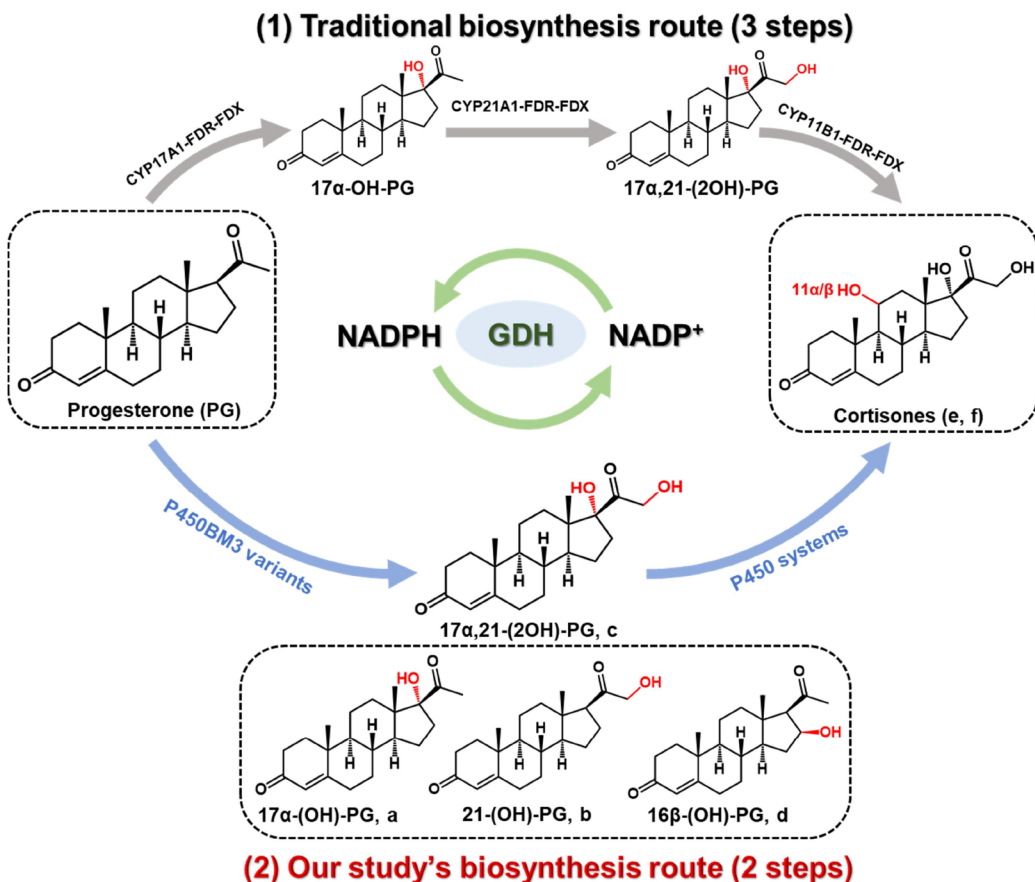
Revised: February 8, 2024

Accepted: February 22, 2024

Published: March 4, 2024



Scheme 1. Converting PG into e/f by “Traditional Route” or “Our Study’s Route”



process and significantly reducing the operation cost from \$200 per gram to less than \$1.<sup>8,15–17</sup> Notably, PG is 10-fold cheaper than *c* and can be biosynthesized *de novo* in a more environmentally friendly process using glucose as substrate in microbial hosts.<sup>18–20</sup> Therefore, synthesis of hydrocortisone using PG as the substrate appears to be a more ecofriendly and cost-effective biosynthetic approach.

Traditional biosynthetic pathways for converting PG into hydrocortisone comprise three steps: (1) CYP17A1 catalyzes the hydroxylation of PG at C17, resulting in the formation of 17 $\alpha$ -hydroxy-PG (*a*)<sup>21</sup>; (2) *a* is hydroxylated by CYP21A2 and converted into 17 $\alpha$ ,21-dihydroxy-PG (cortexolone, *c*)<sup>22,23</sup>; and (3) CYP11B1 hydroxylates C11 of *c* into 11 $\alpha/\beta$  hydrocortisone.<sup>15,17</sup> However, this multistep hydrocortisone synthesis process possesses inherent challenges, including low enzymatic activity of P450s, the complex interplay with cytochrome P450 reductases (CPR) required by the three P450s, lack of coordination in multienzyme cascade reactions, and accumulation of undesirable byproducts.<sup>24</sup> It must be noted that the self-sufficient CYP102A1 (P450BM3) from *Bacillus megaterium* could be expressed on a gram scale in *E. coli*.<sup>6,11,25</sup> In addition, a P450BM3-F87A-V78W-A82F variant, inherently comprising a reductase domain, could produce 4% *c* at an 81% conversion rate.<sup>25</sup> Thus, P450BM3 possesses the engineering potential for one-step production of *c*, and the biosynthetic pathway for hydrocortisone using PG as a substrate can be simplified into a more streamlined two-step process (Scheme 1), without the need for complex multiple CPR matching.

The development of a highly efficient and selective dual-hydroxylating P450BM3 variant at C17 and C21 is crucial to achieve a two-step synthesis of hydrocortisone from PG.<sup>26</sup> Although scanning glycine mutagenesis and scaffold sampling are effective approaches for rationally designing P450s to precisely oxidize steroids, none of the P450BM3 variants are found to efficiently and selectively oxidize C17, C21, and C17/21 of PG.<sup>14</sup> The CYP11A1 catalytic process has been noted to involve concurrent hydroxylation at both C20 and C22 of cholesterol, with both C20 and C22 within 4.6–5.6 Å to the heme center.<sup>18</sup> Thus, the P450 variants for *c* production can be obtained by adjusting the relative distances of C17/C21 of PG from heme's Fe=O through mutation of residues in the heme domain. Additionally, the synthesis of hydrocortisone involves installing multiple oxidations on a single compound. The heme center of P450 is linked to the reaction solvent through channels, facilitating the internal transport of substrates within the protein.<sup>14,27</sup> Li et al.<sup>28</sup> reshaped the bottleneck and the entrance of BM3's substrate access channel for highly regioselective and active p-hydroxylation of m-alkylphenols. Acevedo-Rocha et al.<sup>29</sup> further discovered that interactions within the loops, helices, and  $\beta$ -strands in the substrate access channel of P450BM3 affect the efficiency of substrate entry into the heme center, thereby affecting the efficiency of hydroxylating steroids. Thus, engineering the substrate access channel of P450BM3 can enhance catalytic efficiency and diversify the oxidation of steroids.<sup>27,30</sup> Moreover, computational simulation techniques can be utilized to decipher the potential functions of individual residues within enzyme–substrate complexes, providing impetus for precision-driven

**Table 1.** Hydroxylated Products Obtained from P450BM3 Mutations<sup>a</sup>

P450BM3 mutations	conv.	a	b	c	d	others
first generation mutations						
F87 V	10.4%			2%	59%	28.6%
F87G	11.5%		15%		78%	3%
F87A (1)*	13.6%		1%		67%	32%
second generation mutations						
F87A/P25 V	34.4%		38.7%		61.3%	
F87A/P25G	28.4%		38%		59%	3%
F87A/P25A (2-1)*	40.1%				65.8%	34.2%
F87A/P25A/P329 V	63.2%		41.5%		58.5%	
F87A/P25A/P329G	55%		31.5%		68.5%	
F87A/P25A/P329A (2-2)*	75.3%		14.2%		85.8%	
F87A/P25A/P329A/E435 V	10.3%				60.8%	39.2%
F87A/P25A/P329A/E435G	16.3%		37.2%		62.8%	
F87A/P25A/P329A/E435A	15.3%		39%		61%	
F87A/P25A/P329A/E435D (VD-BM3)*	96.7%		50.6%		47.4%	2%

<sup>a</sup>Screening-scale reactions (500 μL) were performed in 96-well plates containing 100 mM phosphate buffer (pH = 8.0) and 200 mg/L P450BM3 variant. To initiate the reaction, 1 mM PG, GDH (20 U/mL), glucose (100 mM), and NADP<sup>+</sup> (40 μM) were added to the plates and incubated at 25 °C and 220 rpm for 24 h. \* denotes variants in the initial screening library.

enzyme engineering<sup>31,32</sup> and computational simulation-driven refinement in P450 engineering can offer efficient targeted oxidation components for the two-step transformation of PG into hydrocortisone.

In this study, efficient catalytic systems for the two-step synthesis of 11α/β-hydrocortisone (*f,e*) from PG were constructed based on computational simulation guided P450BM3 (CYP102A1 from *B. megaterium* ATCC 14581) engineering. It must be noted that B-factor-guided substrate channel remodeling, molecular docking, and free energy-guided catalytic pocket modification of P450BM3 have expanded the hydroxylation carbon positions of PG to include C16 (*d*), C17 (*a*), and C21 (*b*), and dihydroxylation at C17/21 (*c*). By combining the analysis of CYP5311B2<sup>15</sup> and LG23<sup>6</sup> with computational simulations, a novel P450BM3 variant was rationally redesigned by substrate channel switching for C11α hydroxylation of *c*. The computational simulation-guided P450 engineering strategies can enrich the regioselective hydroxylation of steroids and streamline the process of corticosteroid synthesis from PG into two steps with high efficiency.

## 2. RESULTS

**2.1. Engineering Substrate Access Channel of P450BM3 for PG Hydroxylation.** Efficient access of the substrate into the heme pocket is vital for the P450BM3 catalytic process.<sup>28</sup> The initial P450BM3 engineering strategy aimed to expand the substrate entry to facilitate access of PG to the heme center. It has been noted that the wild-type (WT)-P450BM3 cannot hydroxylate PG (Table 1).<sup>33</sup> The docking result of PG posed in the substrate access channel of WT-P450BM3 showed that F87 obstructs the inert C–H bond of PG from accessing the heme center, thereby hindering subsequent hydroxylation (Figure 1A, B). Consequently, the F87A variant produced 67% 16β-hydroxy-PG (*d*) and 33% 2β-hydroxy-PG at a 13.6% conversion rate (Table 1). However, the large conformationally rigid residues in the substrate access channel of P450BM3 still obstructed the access of PG to the heme center.

We subsequently engineered the substrate access channel of P450BM3-F87A. The Debye–Waller factor (B-factor) offers insights into the mobility and flexibility of atoms, residue side

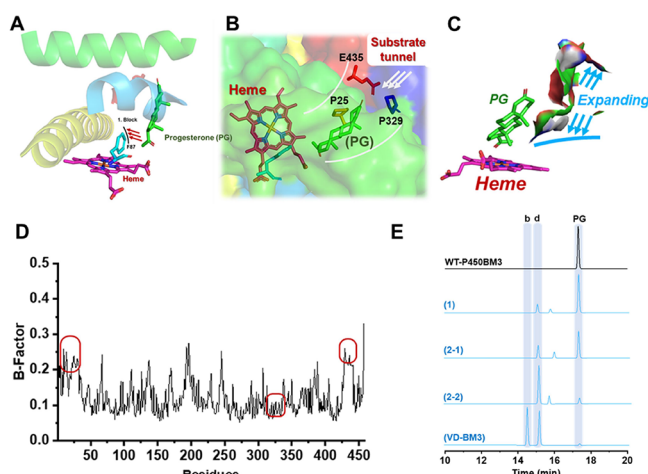


**Figure 1.** Engineering substrate access channel of P450BM3 for PG hydroxylation. (A) WT-P450BM3 docked with PG (green) showing clashes with F87 (blue). WT-P450BM3 is only represented by three Alpha spirals (yellow, blue, and green) and a heme center (red). (B) E435 (red), P25 (blue), and P329 (yellow) of WT-P450BM3 are the inhibitory residues of the entry channel which prevent the access of PG to the heme center. (C) Comparison of substrate access channels between VD-BM3 (white) and P450BM3 (green). (D) B-Factor analysis of each residue of the WT-P450BM3 and PG complexes. The B-factor values for each residue were analyzed using MD simulations in 100 ns. E435, P25, and P329, marked in red circles with B-factor fluctuations of less than 0.02 nm, were selected for substrate access channel engineering. (E) HPLC analysis of PG oxidation by P450BM3 variants.

chains, and loop regions within proteins.<sup>28,34</sup> Therefore, MD simulation was performed with PG docked in the P450BM3-F87A in 100 ns, and the B-factor values of each residue were further analyzed. P25, P329, and E435 from the F87A mutation, all with a conformational range and RMSF fluctuation less than 0.05 nm were selected for further engineering into small conformational residues (Figure 1C, D). F87A-P25A-P329A variant with small conformational hydrophobic alanine residues exhibited effective performance in substrate channel engineering and yielded a PG hydroxylation conversion rate of 75.3% (Table 1). However, the

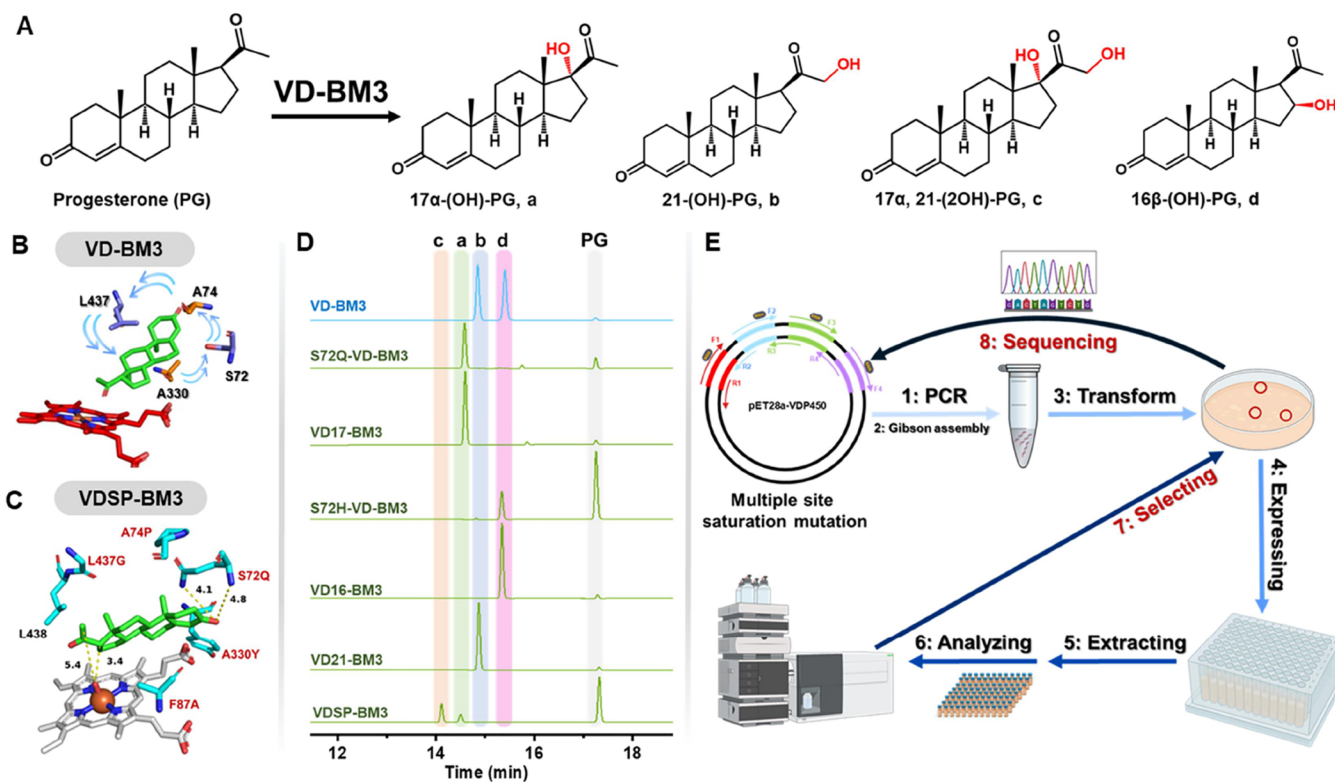


**Figure 2.** Engineering heme pocket of P450BM3 for PG hydroxylation. (A) Engineering of VD-BM3 for catalyzing C17 $\alpha$  (a), C21 (b), C17 $\alpha$ /21 (c), and C16 $\beta$  (d) oxidation of PG. (B) Substrate (PG) docked in VD-BM3. VD-BM3 is only represented by the heme center (red) and residues S72/L437/A330/A74 (purple). S72, L437, A330, and A74 of VD-BM3 regulate the spatial position of the AB rings of PG in the heme center. S72 and L437 are situated on the left and right sides of the AB ring, while A74 and A330 are located above and below the AB ring, respectively. (C) PG docked in VDSP-BM3 for c production. VDSP-BM3 is only represented by the heme center (white) and residues S72Q-A74P-F87A-A330Y-L437G (blue). The distances of C17-FeO and C21-FeO were 3.4 and 5.4 Å, respectively. S72Q formed two hydrogen bonds with PG at distances of 4.1 and 4.8 Å, respectively. (D) HPLC analysis for the oxidation of PG by VD-BM3 variants. (E) Eight-step high-throughput screening of P450 variants. The S72/L437/A330/A74 of VD-BM3 was simultaneously subjected to saturation mutagenesis.

E435A/G/V mutation of P450BM3-F87A-P25A-P329A resulted in a low conversion rate (<16.3%) of PG hydroxylation (Table 1). Subsequently, the F87A-P25A-P329A-E435D variant (VD-BM3) was obtained by saturation mutagenesis of E435, which produced 50.6% *a* and 47.4% *d* at 96.7% conversion rate (Table 1). Following the substrate channel engineering process, the residue properties of VD-BM3 remained unchanged, with only a significant reduction in the conformational size. These results confirmed the achievement of a high conversion rate for PG hydroxylation (Figure 1E); however, the promiscuity of the hydroxylation products of VD-BM3 remains a significant challenge.

**2.2. Initial Engineering of VD-BM3 for Highly Regioselective Oxidation of PG.** VD-BM3, featuring an engineered substrate access channel, has demonstrated a high efficiency in the hydroxylation conversion rate of PG but with poor regioselectivity. An effective strategy to enhance regioselectivity is to rationally engineer residues near the substrate to bring the catalytic group of the substrate closer to the enzyme's active site.<sup>18,35,36</sup> The docking results of PG and VD-BM3 complexes revealed that S72 and L437 were located within a 4-Å range of the AB ring of PG and hence were selected for saturation mutagenesis to recalibrate the distances of the D ring of PG toward the heme center (Figure 2A, B). S72Q-VD-BM3 was capable of producing 97% *a* at an 80% conversion rate (Table 2), while S72H-VD-BM3 produced 97% *d* at a 30% conversion rate. Saturation mutagenesis of

L437 did not yield any VD-BM3 variants with a high regioslective hydroxylation of PG (Table 2). These data clearly demonstrated that the introduction of optimal large conformational residues solely at S72 of VD-BM3 was beneficial in enhancing regioslectivity but reduced the conversion rate of PG hydroxylation. Therefore, L437 of S72Q-VD-BM3 and S72H-VD-BM3 was further mutated into hydrophobic residues with small conformation, respectively. L437G-S72Q-VD-BM3 (VD17-BM3) was found to produce 94% *a* at a 93% conversion rate (Table 2), while L437A-S72Q-VD-BM3 (VD16-BM3) was capable of producing 99% *d* at 96% conversion rate. The smaller conformation of G437 and A437 minimized the hindrance posed by Q72 and H72, resulting in a high conversion rate. However, VD-BM3 variants specifically targeting the production of *b* and *c* could not be generated.

Mutation of only residues S72 and L437 of VD-BM3, located near the AB rings of PG, might not effectively achieve diverse substrate conformations in the heme center to produce *c* (Table 2). Consequently, based on the docking results (Figure 2B), we additionally selected longitudinal residues (A330/A74), also located near the AB rings of PG, for mutation to facilitate *b* and *c* production. Given that VD17-BM3 has already demonstrated high regioslectivity in hydroxyrating C-17 of PG, it holds great potential to be further modified for hydroxyrating C-21 or C-17/21. First, A330 of VD17-BM3 was subjected to saturation mutagenesis,

**Table 2.** Hydroxylated PG was Obtained by VD-BM3 Variants<sup>a</sup>

VD-P450 mutations	conv.	<i>a</i>	<i>b</i>	<i>c</i>	<i>d</i>	others
first generation mutations by one site regulation						
VD-BM3 (Starting P450)	96.7%	47.4%				50.6%
<b>VD-S72Q*</b>	<b>80%</b>	97%				3%
VD-S72C	40%	90%			5%	5%
<b>VD-S72H*</b>	<b>30%</b>				<b>97%</b>	3%
VD-L437G	20%	80%			20%	
VD-L437C	25%	75.3%			12%	12.7%
VD-L437T	21%	66.6%			30%-	3.4%
VD-L437A	27%	50%			30%	20%
second generation mutations by two sites regulation						
<b>VD-S72QL437G* (VD17BM3)</b>	<b>93%</b>	<b>94%</b>				<b>6%</b>
VD-S72QL437C	20%	27%	4%			69%
VD-S72QL437T	45%		20%			80%
VD-S72QL437A	29%	41%			30%	21%
<b>VD-S72HL437A* (VD16BM3)</b>	<b>96%</b>				<b>99%</b>	<b>1%</b>
third generation mutations by multi sites regulation						
VD-S72QL437GA330F	43%	63%		37%		
VD-S72QL437GA330W	83%	21%		75%		4%
<b>VD-S72QL437GA330Y*</b>	<b>11%</b>	<b>10%</b>	<b>5%</b>	<b>85%</b>		
VD-S72QL437GA330H	20%	30%				70%
VD-S72QL437GA330YA74I	13%	15%	30%	20%		35%
<b>VD-S72QL437GA330YA74G*(VD21BM3)</b>	<b>96%</b>	<b>5%</b>	<b>95%</b>			
VD-S72QL437GA330YA74P*(VDSBPBM3)	40%	35%	3%	62%		
VD-S72QL437GA330YA74 V	12%	16%	3%	40%		41%
VD-P450 mutations						
VD-S72QL437GA330YA74F	37%	40%	1%	20%		39%
VD-S72QL437GA330YA74I	17%	60%				40%
VD-S72QL437GA330YA74Y	29%			67%		33%
VD-S72QL437GA330YA74W	11%		90%	10%		
fourth generation mutations by multiple site saturation mutation						
VD-Q72G-G437A-Y330F-P74	85%	35%		30%		35%
VD-Q72-G437-Y330G-A74F	60%	25%	25%	50%		
VD-Q72A-G437 V-Y330-A74G	53%	20%	40%	40%		
VD-Q72H-G437-Y330F-A74G	42%	35%		25%	40%	
VD-Q72H-G437F-Y330G-A74G	87%	46%	3%	51%		

<sup>a</sup>Screening-scale reactions (500  $\mu$ L) were performed in 96-well plates containing 100 mM phosphate buffer (pH 8.0) and 200 mg/L P450BM3 variant. To initial the reaction, 1 mM PG, GDH (20 U/mL), glucose (100 mM), and NADP<sup>+</sup> (40  $\mu$ M) were added and incubated at 25 °C and 220 rpm for 24 h. \* denotes variants in the initial screening library. P450 variants with a conversion rate exceeding 10 and 40% were obtained in first–third and fourth generation, respectively.

and the A330Y variant could produce 85% *c* at a 11% conversion rate (Table 2). Subsequently, A74 of **VD17-BM3**-A330Y was subjected to saturation mutagenesis (Table 2), and the A74P variant (**VDSBPBM3**) could produce 62% *c* at a 40% conversion rate (Figure 2C). Moreover, **VD17-BM3**-A330Y-A74G (**VD21-BM3**) was found to produce 95% *b* at a 96% conversion rate. Despite obtaining a series of P450 variants capable of efficiently synthesizing *a*, *b*, and *d* through conformational changes to residues 72, 74, 330, and 437 in **VD-BM3**, the production of *c* remained constrained by low conversion rates (<40%) (Figure 2D). Given that S72/L437/A330/A74 of **VD-BM3** was individually subjected to saturation mutagenesis, some effective variants may have been overlooked owing to the limited size of the mutation library. Consequently, we simultaneously subjected the four residues of S72/L437/A330/A74 to saturation mutagenesis (Figure 2E), which resulted in  $20^4$  variants, representing a substantial workload. Therefore, we assessed only 1920 variants and identified five **VD-BM3** variants producing *c* with a conversion rate exceeding 40% (Table 3). Furthermore,

we found that the incorporation of rigid residues along with smaller conformational residues (alanine and glycine) could significantly enhance the conversion rate (Table 2). However, this strategy was constrained by a significant reduction in regioselectivity (<50% for *c*) and the extensive number of P450 variants required for screening.

**2.3. Free Energy Calculation-Guided P450 Engineering for *c* Production.** Although **VDSBPBM3**, featuring modifications in the heme center, can synthesize *c* with high regioselectivity, its conversion rate remains low. To explore the reasons for the low conversion rates of **VDSBPBM3**, both **VD-BM3** with a 96.7% conversion rate and **VDSBPBM3** were comprehensively analyzed by MD simulation for 100 ns. As shown in Figure 3B, the fluctuation range of the B-factor value for **VD-BM3** was significantly higher than that for **VDSBPBM3**, indicating that the pocket of **VDSBPBM3** was more rigid than that of **VD-BM3**. In the **VD-BM3** engineering process, the appropriate introduction of a combination of rigid and flexible residues was found to significantly enhance the conversion rate and selectivity of P450. Therefore, the protein secondary

**Table 3. Conversion of Hydroxylated PG to *c* by a Flexible VDSP-BM3 Catalytic Pocket<sup>a</sup>**

VD-P450 mutations	conv.	<i>c</i>	others
<b>Template_VD-S72QL437GA330YA74P*</b>	40%	62%	38%
VD-S72QL437GA330YA74P-R66G	55%	25%	75%
VD-S72QL437GA330YA74P-I259G	30%	26%	74%
VD-S72QL437GA330YA74P-F261G	20%		100%
VD-S72QL437GA330YA74P-E267G	20%		100%
VD-S72QL437GA330YA74P-V317G	67%	50%	50%
VD-S72QL437GA330YA74P-L324G	20%	66%	40%
VD-S72QL437GA330YA74P-T327G	5%	61%	39%
VD-S72QL437GA330YA74P-E348G	30%	25%	10%
VD-S72QL437GA330YA74P-A399G	39%	10%	90%
VD-S72QL437GA330YA74P-A406G	38%	10%	90%
VD-S72QL437GA330YA74P-Y429G	68%	22%	78%
<b>VD-S72QL437GA330YA74P-D432G</b>	70%	70%	30%
<b>VD-S72QL437GA330YA74P-K434G</b>	72%	72%	28%
VD-S72QL437GA330YA74P-D435G	2%	71%	29%
VD-S72QL437GA330YA74P-L439G	71%	60%	40%
<b>VDS72QL437GA330YA74P-D432GK434G*</b>	89%	85%	15%
VDS72QL437GA330YA74P-D432GK434GL439G	50%	72%	28%

<sup>a</sup>Screening-scale reactions (500 μL) were performed in 96-well plates containing 100 mM phosphate buffer (pH 8.0) and 200 mg/L P450BM3 variant. To initiate the reaction, 1 mM PG, GDH (20 U/mL), glucose (100 mM), and NADP<sup>+</sup> (40 μM) were added and incubated at 220 rpm and 25 °C for 24 h. \* denotes variants in the initial screening library.

structures near the PG in the pocket of **VDSP-BM3** were further analyzed and categorized into five domains (Figure 3A). However, as mutation of all residues in these five regions constitutes a substantial workload, we employed the gmx\_mmPBSA script to calculate the free energy of each residue in the five structural domains.<sup>37</sup> Based on the results obtained, residues R66 (Region 4), I259–F261–E267 (Region 5), V317–L324–T327–E348 (Region 3), and A399–A406–Y429–D432–K434–D435–L439 (Region 1), exhibiting repulsive forces (with high positive free energy values), were selected for mutation (Figure 3C). Glycine scanning represents an effective strategy for enhancing the flexibility of the P450 catalytic pocket.<sup>4</sup> Hence, all of the aforementioned residues were individually mutated into glycine, as detailed in Table 3. Finally, the D433G-K435G-VDSP-BM3 variant (**VD1721-BM3**) exhibited a significantly improved conversion rate from 40 to 89% and increased regioselectivity from 62 to 85% for *c* production. Furthermore, PG was also docked with **VD1721-BM3**, and the optimal docking complexes underwent a 100-ns MD simulation. D433G-K435G led to an increase in B-factor fluctuations in regions 2 and 3 of **VD1721-BM3** (Figure 3B), and the enlargement of the catalytic pocket facilitated an increase in the conversion rate for *c* production from 40 to 89%. The distances between C17 and C21 from Fe=O of the heme center were noted to be approximately 3.5 and 3 Å, respectively (Figure 3B). These nearly equivalent distances ensured efficient production of 17*α*,21-dihydroxy-PG.

**2.4. Switching Substrate Access Channel of P450 for *e* and *f* Production.** Obtaining P450s capable of hydroxylating the C11 of *c* is crucial to the synthesis of *e* and *f* (Figure 4A). Through natural evolution, AoCYP5311B2 and its AoCPR from the zygomycete fungus *Absidia orchidis* are well-known for their steroid 11*β*-hydroxylation capability and have been widely utilized in the biotransformation of

hydrocortisone.<sup>22,23</sup> CYP5311B2 and its CPR have been validated for their biological activity in *Saccharomyces cerevisiae*.<sup>15</sup> Therefore, the AoCYP5311B2-AoCPR catalytic system (pETDuet-CYP5311B2-CPR) was introduced into *E. coli* BL21(DE3), which produced 91% hydrocortisone (**11β,e**) and 9% 11*α*-hydrocortisone (*f*) with a 93% conversion rate (Table 4). Thus, we obtained efficient CYP5311B2-CPR for *e* production.

It has been reported that LG-23, characterized by R47W–S72W-F77Y–V78L-F81I-A82L-F87G-T88S-M177T-M185Q–L188Q-I209T-A328G-A330W-T438S mutations of P450BM3, exhibits high regioselectivity in hydroxylating the C11*α* of estra-4,9-diene-3,17-dione.<sup>8,38</sup> Consequently, we utilized LG-23 to convert 1 mM *c* into *e* or *f* and obtained 97% *f* with a 40% conversion rate (Table 4). As **VD-BM3** generated in the present study did not exhibit C11 hydroxylation activity for the production of *c*, we docked PG into **LG-23** and **CYP5311B2**, respectively, and analyzed the differences in the catalytic processes (Figure 4B, C). Unlike **VD-BM3**, **LG-23** can obstruct the substrate channel by introducing W47, W72, and W330, which have larger conformations, and facilitate substrate access predominantly from the loop region composed of L324–G328 by incorporating G328 (Figure 4C). Furthermore, the substrate can enter the heme domain of **VD-BM3** diagonally from the top right, leading to a preference in P450 variants for producing 2*β*, 16*β*, 17*α*, and 21-hydroxy-PG. Thus, the conformation of the substrate access channel is a critical factor influencing the regioselective hydroxylation sites of P450s. Accordingly, we redesigned P450BM3 for hydrocortisone bioproduction by switching the substrate access channel (Figure 4D). Initially, starting from P450BM3-F87A, A328G was introduced for opening a new substrate access channel. P450BM3-F87 V-A328G (**FA-BM3**) could hydroxylate *c* with a 20% conversion rate (Table 4). Subsequently, P25, S72, and A330 of **FA-BM3** were mutated into bulky residues for blocking the original substrate access channel. The **FA-BM3**-P25F variant demonstrated the ability to hydroxylate *c* with a 35% conversion rate but did not produce *e* or *f*. The docking results between **LG-23** and the *c* complex revealed that the residues W72 and W330 helped in exposing C11 above the heme center (Figure 4C, D). Thus, S72W-A330W was introduced into **FA-BM3**-P25 for facilitating exposing C11 of *c* above the heme center, which could produce 92% *c* at a 58% conversion rate (Figure 4D). In fact, the new substrate access channel with G328 requires further flexibilization of other residues within the channel to achieve a higher conversion rate. During the process of generating **VD1721-BM3**, the flexibility of domain 1 (D433-L439 loop region) was found to significantly improve the conversion rate. In fact, domain 1 was also located in the new substrate channel (Figure 4D) and was further selected for glycine scanning (Table 4). Finally, the **FA-BM3**-P25F–S72W-A330W-L437G-L439G variant (**FA11a-BM3**) could produce 90% *c* at an 85% conversion rate (Table 4). When compared with the less accommodating substrate channel surface (marked white in Figure 4C) of **VD-BM3**, A328G, L437G, and L439G in **FA11a-BM3** produced larger, more accommodating channel surfaces (marked green in Figure 4E), facilitating the access of substrate *c* to the heme center. In addition, the rigid conformations of A330W and S72W enhanced the exposure of the C11 position of *c* above the heme center with a distance of 4.5 Å (Figure 4F). Once *c* entered the heme center, extensive hydrogen bond interactions with A87, T260, I263,

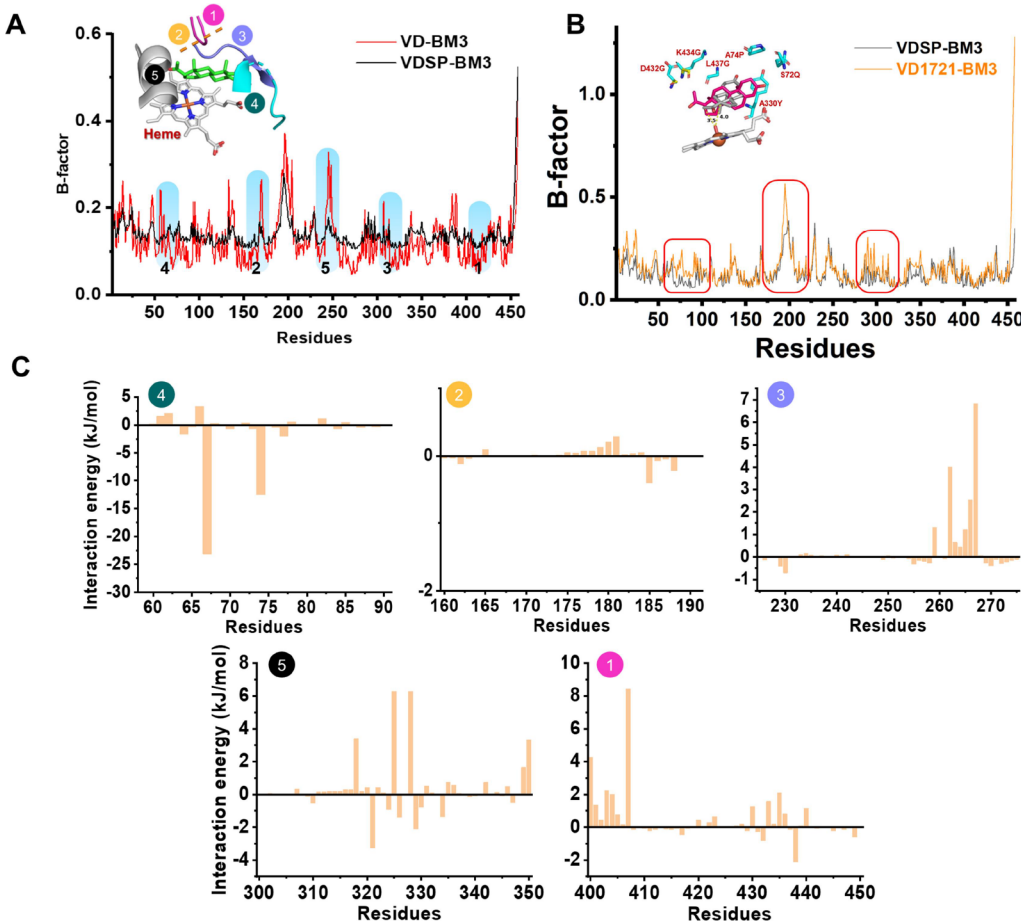


**Figure 3.** MD simulation analysis of VD-BM3, VDSP-BM3, and VD1721-BM3. (A) B-Factor analysis of VD-BM3/PG and VDSP-BM3 complexes by using MD simulation in 100 ns. PG docked in VDSP-BM3 for *c* production. Five regions and heme center of VDSP-BM3 are presented: 1: Purple area, residues 400–450; 2: Yellow area, residues 160–190; 3: Blue area, residues 300–350; 4: Green area, residues 60–90; 5: Black area, residues 400–450. (B) B-Factor analysis of VDSP-BM3/PG and VD1721-BM3 complexes using MD simulation for 100 ns. PG docked in VD1721-BM3 for *c* production. VD1721-BM3 is only represented by the heme center (white) and residues S72Q-A74P-A330Y-D433G-K435G-L437G (blue). (C) Free energy calculation for each residue in the five regions. Residues R66 (Region 4), I259–F261-E267 (Region 5), V317-L324-T327-E348 (Region 3), and A399-A406-Y429-D432-K434-D435-L439 (Region 1) exhibited repulsive forces with high positive interaction energy values (kJ/mol).

T268, and A328 contributed to stable hydrogen bonds, featuring distances of 3.0, 2.6/4.0, 3.1, 3.8, and 3.4 Å, respectively (Figures 4F and S7C). Finally, we obtained efficient FA11a-BM3 for *f* production.

**2.5. Analysis of Mechanism Underlying High Regioselectivity and Conversion Rates of P450 Variants.** Computation-aided P450 engineering facilitated the development of VD16-BM3, VD17-BM3, VD21-BM3, and VD1721-BM3 for steroidal core hydroxylation. All of the five purified P450BM3 variants were utilized to analyze the enzyme kinetic parameters (Table S1) and exhibited efficient catalytic activity ( $k_{\text{cat}}/K_m > 171.45 \mu\text{M}^{-1} \text{S}^{-1}$ ) (Figures S1–S5). To elucidate the mechanism underlying the high regioselectivity and conversion rates of the five P450BM3 variants, extensive structural and computational analyses were conducted by using molecular docking and molecular dynamic simulation.

VD16-BM3 and VD17-BM3 were obtained by engineering S72 and L437 of VD-BM3 and exhibited high selectivity on the oxidation of C16 and C17 of PG, respectively. The H72 of VD16-BM3 restricted the original conformation AB rings of PG (shown in blue) downward and eliminated the hydrogen bond interaction initially exhibited by S72 of VD-BM3 (Figure

S5A). Furthermore, A437 expanded a larger hydrophobic space, enabling PG to shift toward the bond direction (shown in blue). The MD simulation also revealed that the distance between C16 of PG and Fe=O of VD16-BM3 was approximately  $2.8 \pm 0.3$  Å over 100 ns. The position of PG (shown in yellow) in VD17-BM3 was parallel to that of the heme, and S72Q of VD17-BM3 formed a hydrogen bond with C3 of PG within 5.0 Å, stabilizing the position of PG in the heme center (Figure S5B). Similar to the VD16-BM3-catalyzed 16 $\beta$ -hydroxylation, G437 of VD17-BM3 also generated a larger hydrophobic space to accommodate the AB rings of PG (Figure S5B). The MD simulation of VD17-BM3 and PG complexes revealed that the distance between C17 of PG and Fe=O was approximately  $3.0 \pm 0.6$  Å over a 100-ns period. VD21-BM3 was obtained by engineering A74 and A330 of VD17-BM3 and exhibited high selectivity on the oxidation of C21 of PG. The Y330 of VD21-BM3 formed a hydrogen bond and  $\pi$ – $\pi$  stacking interaction with the A ring of PG at distances of 4.7 and 4.8 Å, respectively (Figure S5C). In addition, G74 formed a weaker hydrogen bond with PG at a distance of 5.9 Å. However, as Y330 in the heme center produced an extremely rigid conformation, the Q72, G74, and G437 of

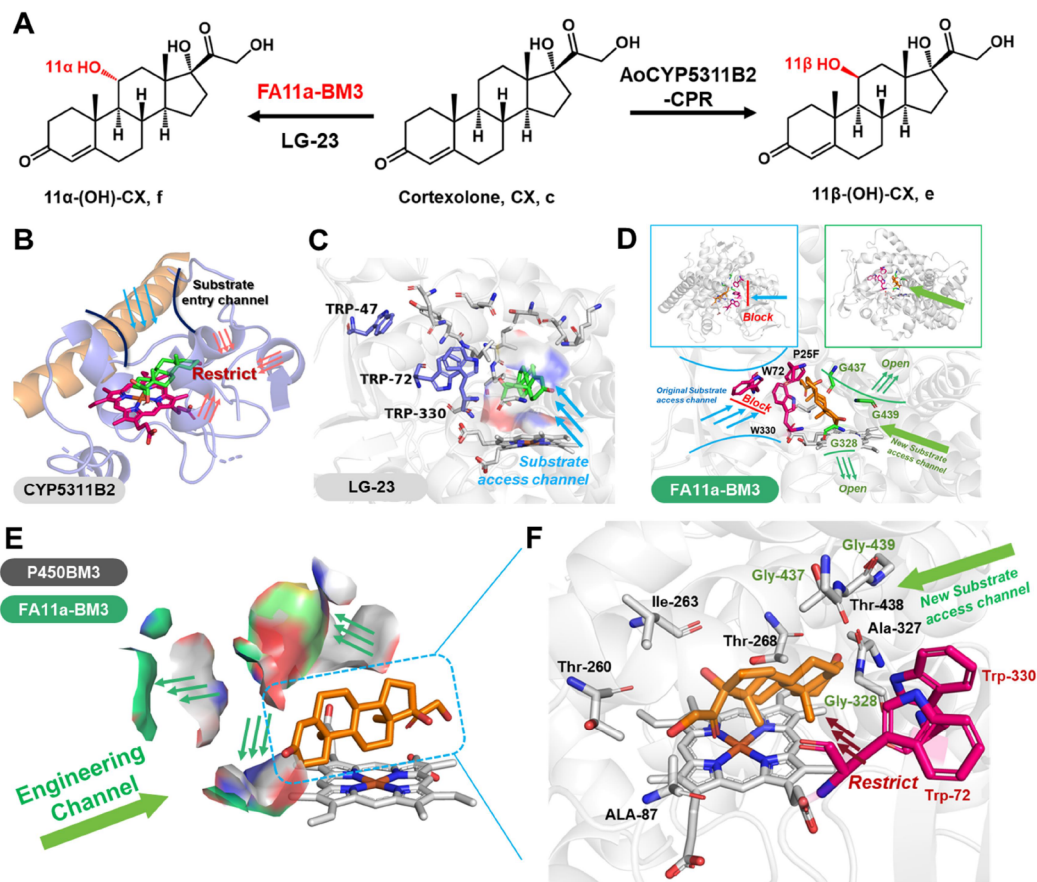


**Figure 4.** Switching substrate access channel of P450 for *e* and *f* production. (A) Constructing P450 systems for *e* and *f* production. (B) Docking of *c* in CYP5311B2 for *f* production. Blue arrows indicate the entry of *c* into the substrate channel. (C) Docking of *c* in LG-23 for *f* production. Blue arrows indicate the entry of *c* into the substrate channel of LG-23. TRP-47, TRP-72, and TRP-330 (blue) promote C11 of *c* (green) to be exposed above the heme center (white). (D) Overall process of the FA11a-BM3 functional modification. F25, W330, and W72 play roles in blocking the original substrate access channel (red). G328, G437, and G439 in FA11a-BM3 create a larger, more accommodating substrate access channel (green). (E) Substrate channel surfaces of P450BM3 (gray) and FA11a-BM3 (green). Green arrows denote the direction of expansion. (F) Docking of *c* (yellow) in the FA11a-BM3 heme pocket (white). The residues (white) forming interactions within a range of 5 Å near *c* in the heme center are shown.

**Table 4.** Hydroxylated *c* Obtained by Rational Engineering of P450BM3<sup>a</sup>

P450	conv.	<i>e</i>	<i>f</i>	others
CYP5311B2-CPR	93%	91%	9%	
LG-23	40%		97%	3%
F87 V-P450BM3				
<b>F87 V-A328G (FA-BM3)</b>	20%		100%	
FA-BM3-P25F	28%		100%	
FA-BM3-P25F-A330W	35%		100%	
FA-BM3-P25F-A330W-S72W	58%	92%	8%	
FA-BM3-P25F-A330W-D432G	20%		100%	
FA-BM3-P25F-A330W-S72W-K434G	25%	99%	1%	
FA-BM3-P25F-A330W-S72W-E435G	35%		100%	
FA-BM3-P25F-A330W-S72W-L437G	71%	93%	8%	
FA-BM3-P25F-A330W-S72W-L439G	65%	88%	12%	
<b>FA-BM3-P25F-A330W-S72W-L437G+L439G (FA11a-BM3)</b>	85%	90%	10%	

<sup>a</sup>Screening-scale reactions (500 μL) were performed in 96-well plates containing 100 mM phosphate buffer (pH 8.0) and 200 mg/L P450BM3 variant. To initiate the reaction, 1 mM *c*, GDH (20 U/mL), glucose (100 mM), and NADP<sup>+</sup> (40 μM) were added and incubated at 220 rpm and 25 °C for 24 h. \* denotes variants in the initial screening library.

**VD21BM3** (highlighted in blue) were utilized to expand the movable space of PG in three distinct directions (Figure 5C). The MD simulation of **VD21-BM3** and PG complexes revealed that the distance between C21 of PG and Fe=O was approximately  $2.9 \pm 0.8$  Å over a 100 ns period.

**VD1721-BM3** was engineered by increasing the flexibility of the heme catalytic pocket in **VDSP-BM3**. The residues Q72, P74, and Y300 with rigid conformation in **VDSP-BM3** regulated C17 and C21 of PG (shown in red) positioned 3.4 and 5.4 Å away from Fe=O, respectively (Figures 2B and 5D). Consequently, the introduction of G433 and G435 in **VD1721-BM3** expanded the hydrophobic space (in the direction of the blue arrow), causing a shift in the AB rings of PG (shown in gray) toward the additional space (Figure 5D). The MD simulation results also revealed that the overall *B*-factor fluctuations in **VD1721-BM3** were higher than those in **VDSP-BM3** (Figure 4E). The residues in flexible region 1 significantly alleviated the compression exerted by Q72, P74, and Y300 of **VD1721-BM3** on the steroid conformation. As a result, the distances between C21/C17 of PG and Fe=O in **VD1721-BM3** were approximately  $3.7 \pm 0.5$  and  $3 \pm 0.3$  Å, respectively. These nearly equal distances endowed **VD1721-BM3** with a higher dual hydroxylation capability at C17/21, when compared with **VDSP-BM3**.

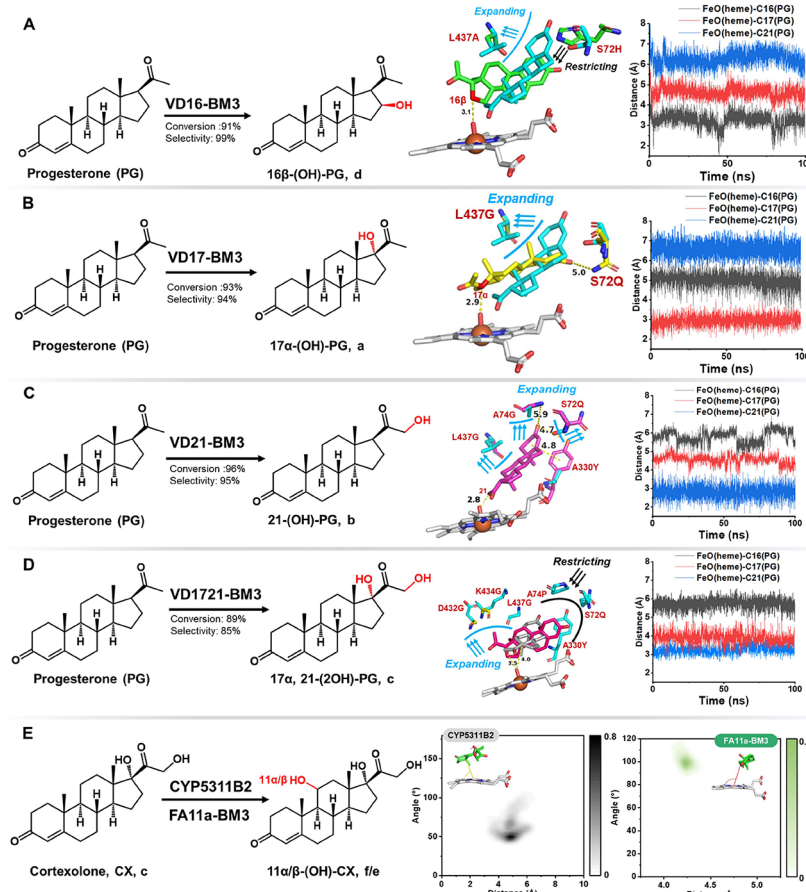


**Figure 5.** Mechanism analysis of PG hydroxylation by P450BM3 variants. (A) L: VD16-BM3 catalyzes C16 $\beta$  (red) oxidation of PG. M: VD16-BM3 (green), represented by H72 and A437, docked with PG (green). VD16-BM3 and PG complexes are overlaid with VD-BM3 (cyan) and PG (cyan) complexes. VD-BM3 is represented only by S72 and L437. Blue arrow indicates the direction of pocket enlargement. R: Distances between FeO (heme) of VD16-BM3 and C16/17/21 of PG were measured by MD simulation in 100 ns. (B) L: VD17-BM3 catalyzes C17 $\alpha$  (red) oxidation of PG. M: VD17-BM3 (yellow), represented by Q72 and G437, docked with PG (yellow). Q72 formed a hydrogen bond with PG (yellow) at a distance of 5.0 Å. R: Distances between FeO (heme) of VD17-BM3 and C16/17/21 of PG were measured by MD simulation in 100 ns. (C) L: VD21-BM3 catalyzes C21 oxidation of PG. M: VD21-BM3 (purple), represented by Q72, G74, Y330, and G437, is docked with PG (purple). Y330 formed an  $\pi$ - $\pi$  stack with PG at a distance of 4.8 Å. Y330 and Q72 also formed hydrogen bonds with PG. R: Distances between FeO (heme) of VD21-BM3 and C16/17/21 of PG were measured by MD simulation in 100 ns. (D) L: VD1721-BM3 catalyzes C17 and C21 oxidation of PG. M: VDSP-BM3 (cyan), represented by Q72, P74, Y330, D432, K434, and G437, is docked with PG (purple). VD1721-BM3 (yellow), represented by G432 and K434, is docked with PG (gray). Black arrow denotes the direction of restriction by Q72, P74, and Y330. R: Distances between FeO (heme) of VD1721-BM3 and C16/17/21 of PG were measured by MD simulation in 100 ns. (E) L: CYP5311B2 and FA11a-BM3 catalyzed C11 $\beta$  and C11 $\alpha$  oxidation of PG. The distances between C11-c and Fe-heme and the angles of C11(c)-Fe(heme)-C1(heme) over a period of 100 ns, respectively. M: CYP5311B2. R: FA11a-BM3. Notes: Conversion rate and selectivity rate for hydroxylation of 1 mM PG by VD-BM3 variants were obtained in 24 h. (A) VD16-BM3; (B) VD17-BM3; (C) VD21-BM3; (D) VD1721-BM3; (E) CYP5311B2 and FA11a-BM3. L, M, and R denote left, middle, and right, respectively.

CYP5311B2 and FA11a-BM3, obtained in this study, exhibited high selectivity on the oxidation of C11 $\beta$  and C11 $\alpha$  of *c*, respectively. The docking results additionally indicated that *c* is located nearer the  $\alpha$  helix in the heme center of CYP5311B2 than that of FA11a-BM3. Subsequently, we measured the distances between C11-*c* and Fe-heme and the angles of C11(*c*)-Fe(heme)-C1(heme) over a period of 100 ns, respectively (Figure 5E). The distances between C11 of *c* and the FE values of CYP5311B2 and FA11a-BM3 are both around 4 Å. When the C11 of *c* and Fe form an acute angle, this configuration is associated with increased C11 $\beta$  hydroxylation, while an obtuse angle is linked to enhanced C11 $\alpha$  hydroxylation (Figure 5E). To explain the angle changes of C11-*c* and Fe in CYP5311B2 and FA11a-BM3, the *B*-Factor of CYP5311B2 and FA11a-BM3 were further analyzed, respectively. In fact, *B*-factor values of the long  $\alpha$  helix near

heme in CYP5311B2 (residues from 315 to 346) are significantly higher than in FA11a-BM3 (residues from 252 to 283), indirectly indicating that the naturally more flexible  $\alpha$  helix in CYP5311B2 can facilitate closer substrate proximity (Figure S6A). Additionally, we also found that D397 in CYP5311B2 could form a hydrogen bond with *c* at distances of 3.0 Å (Figure S6B), which enabled CYP5311B2 to better catalyze the C11 $\beta$  hydroxylation of *c*.

**2.6. Two-Step Biosynthesis of Hydrocortisone from PG.** A novel whole-cell catalytic system for the biosynthesis of hydrocortisone from PG was developed, which comprised VD1721-BM3 and FA11a-BM3 (**System1**) or VD1721-BM3 and CYP5311B2-CPR (**System2**), and constructs pETDuet-VD1721BM3-FA11aBM3 and pETDuet-VD1721BM3-CYP5311B2-CPR were developed (Figure 6A). In addition, the pACYCDuet-GDH construct was developed to express

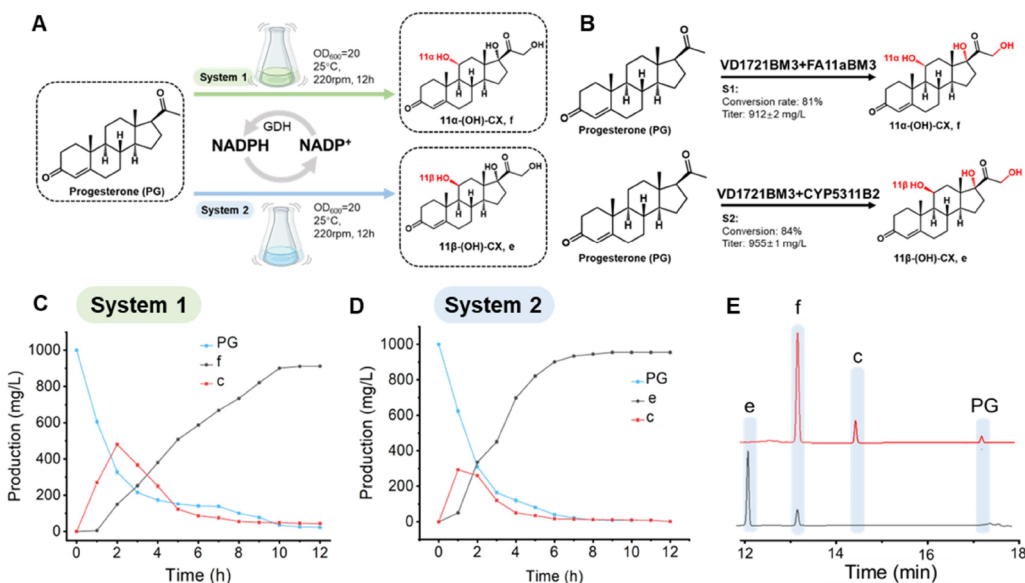


**Figure 6.** Whole-cell catalytic system for *e* and *f* production. (A) Biosynthetic route for conversion of PG to *e*/*f*. NADPH were generated by GDH. System1 contained VD1721-BM3 and FA11a-BM3. System2 contained VD1721-BM3 and CYP5311B2-CPR. *E. coli* with expressing P450s were all resuspended to  $OD_{600} = 20$ . (B) Conversion rate and selectivity rate for PG to *f* and *e* in System1 (S1) and System2 (S2), respectively. (C) The production of PG, *f*, and *c* by System1 was analyzed in 12 h. (D) The production of PG, *e*, and *c* by System2 was analyzed in 12 h. (E) HPLC analysis for S1 (red) and S2 (black) production after 12 h.

GDH, thereby facilitating the conversion from  $NADP^+$  to NADPH. After the expression was induced in *E. coli*, the bacteria were uniformly collected and resuspended to an  $OD_{600}$  of 20 in a 250-mL conical flask followed by the addition of 1 g/L PG and 1 mM  $NADP^+$ . In **System 1**, both VD1721-BM3 and FA11a-BM3 catalyzed the hydroxylation of PG, yielding 11 $\alpha$ -hydrocortisone with a molar conversion rate of 81% (Figure 6B). In **System 2**, both VD1721-BM3 and CYP5311B2-CPR catalyzed the hydroxylation of PG, yielding 11 $\beta$ -hydrocortisone with a molar conversion rate of 84% (Figure 6B, E). After 12 h, both **System1** and **System2** essentially completed the reactions, yielding  $912 \pm 2$  mg/L 11 $\alpha$ -hydrocortisone and  $955 \pm 1$  mg/L 11 $\beta$ -hydrocortisone, respectively (Figure 6C,D). Notably, the introduction of these highly efficient dual-hydroxylating P450 variants created a powerful catalytic system for synthesizing human hormones such as hydrocortisone. This approach holds significant potential for bridging the gap between stringent synthetic requirements and intrinsic properties of natural enzyme catalysts.

### 3. DISCUSSION

Traditional multistep hydrocortisone synthesis faces inherent challenges, including low enzymatic activity of P450s, complex CYP-CPR network, lack of coordination in multienzyme cascade reactions, and accumulation of undesirable by-products.<sup>8,15,24</sup> The present study indicated that the use of computational simulation strategies to guide P450 enzyme engineering can simplify the mutation library and swiftly generate P450 variants that can catalyze the multistep oxidation of inert substrates. Engineered self-sufficient P450BM3 variants effectively reduced the traditional process of hydrocortisones synthesis from PG to a simplified two-step process involving at least two enzymes.<sup>24</sup>

Engineering of substrate access channels and heme centers of P450s has proved to be an effective strategy for enhancing the efficiency of oxidation of substrates.<sup>15</sup> The *B*-factor and

free energy analysis using MD simulation allows rapid identification of residues that obstruct substrate entry into the protein pocket as well as investigation of the forces exerted by residues within the pocket on the substrate.<sup>34,39,40</sup> Introduction of mutations R47I and R47L in P450BM3 can increase hydrophobicity and expand the channel, thereby facilitating better access of m-alkylphenol to the heme center.<sup>28</sup> Consistent with the findings of this study, P25A-P329A-E435D of VD-BM3 and A328G-L437G-L439G of FA11a1-BM3 can create larger, more accommodating channel surfaces that facilitate the access of more steroids to the heme center. However, the substrate channels are often composed of numerous hydrophobic residues.<sup>41</sup> The present study proved that rational selection of obstructive residues through *B*-factor analysis is an effective strategy for substrate channel engineering. In fact, the *B*-factor has been extensively elucidated and applied in studying enzymes, particularly in identifying and interpreting rigidity, flexibility, and internal movements.<sup>34,38</sup> In addition, the properties of the residues were also noted to remain unchanged after substrate channel engineering. In particular, engineering E435 into hydrophobic nonpolar residues did not result in a higher conversion rate during the engineering process of VD-BM3, whereas a smaller conformation, E435D, caused increased catalytic activity. Modification of enzyme surface residues to other types may disrupt the surface charge and further affect the catalytic efficiency.<sup>42</sup> Overall, the *B*-factor analysis can reduce the number of candidate residue mutations in substrate channel engineering and further streamline the types of mutations at each residue by replacing the residues with others presenting similar properties. Natural or artificial evolution of the substrate access channel can, respectively, adjust the direction of substrate entry into the CYP5311B2 and FA11a-BM3 heme center, thereby achieving unprecedented hydroxylation sites. In the engineering VD-BM3 substrate access channel process, no variants were found to hydroxylate the  $sp^3C-H$  of PG's or *c*'s BC rings. In fact, the C11 hydroxylation of *c* was achieved by

artificially switching the substrate access channel. Additionally, the rigidity of the long  $\alpha$  helix near the heme center influences the hydroxylation at C11 $\alpha$  and C11 $\beta$  of *c*. The naturally evolved CYP5311B2, with its more flexible  $\beta$  helix, possesses the capability for C11 $\beta$  hydroxylation of *c*.

Engineered P450 variants have been noted to occasionally exhibit high selectivity for oxidizing a single carbon position but show relatively low conversion rates.<sup>4,8,24</sup> In our initial screening, we evaluated at least 2000 P450BM3 variants, encompassing both single-point saturation mutations and multisite combined saturation mutations. However, variants capable of maintaining high selectivity and enhancing the hydroxylation conversion rate of PG at C17/21 were not identified. It must be noted that once the substrate enters the heme center, it encounters varying forces from residues near the pocket.<sup>33,38</sup> For instance, an extensive network of interaction energies can stabilize the substrate's position within the pocket, whereas certain repulsive forces have the potential to invert the spatial orientation of the substrate.<sup>6,11,38,40</sup> These issues can be efficiently addressed by free energy calculations that can refine the interaction energies of pocket residues and obtain effective mutants with a minimally sized mutation library (17 P450 variants).<sup>40</sup> Alternatively, in the present study, glycine scanning for region 1 (A399-L439) yielded favorable results for a high conversion rate during the generation of **VD1721-BM3** and **FA11a-BM3**. Similar to LG23 engineering, the variant LG-23/T438S of region 1 was identified with improved 11 $\alpha$  selectivity (78 → 92%) at 9(10)-dehydronandrolone conversion (>95%).<sup>8</sup> Thus, the rational modification of region 1 in P450BM3 offers a promising strategy for enhancing the efficiency of steroid hydroxylation.

The principle of enzyme engineering involves the generation of enzymes with new functionalities through rational design, serving as efficient catalytic components for the synthesis of target compounds.<sup>31</sup> The CYP450 superfamily of heme-thiolate monooxygenase enzymes are typically anchored to microbial membrane structures and function physiologically in conjunction with the oxidoreductase enzyme CPR.<sup>43</sup> However, corticosteroid synthesis requires the combination of at least three types of CYP450 enzymes with three different CPRs.<sup>24</sup> Such intricate expression of P450s imposes a significant burden on the cell membrane of *E. coli*.<sup>17,23,24</sup> Furthermore, interactions between different CPRs can disrupt their matching with the original CYP450s.<sup>44</sup> This complex network, comprising three types of CYPs and three types of CPRs, presents substantial challenges for the synthesis of downstream products.<sup>44</sup> The highest hydrocortisone production of the traditional biosynthetic route from PG was 6.1 mg/L in Pan et al.'s study.<sup>24</sup> **VD1721-BM3**, a self-sufficient P450BM3 variant engineered in the present study, effectively streamlined the biosynthesis of *c* from PG from a two-step process to a single-step process, reducing the number of CYP450s in the catalytic system from four to just one.<sup>24</sup> **System1** and **System2**, constructed in the present study, essentially completed the reactions, yielding  $912 \pm 2$  mg/L 11 $\alpha$ -hydrocortisone and  $955 \pm 1$  mg/L 11 $\beta$ -hydrocortisone, respectively, which are the current highest reported yields of corticosteroids biosynthesized from PG.<sup>24</sup> The yield of this study is 156 times higher than that of traditional synthetic pathways.<sup>24</sup> Therefore, in the *E. coli* catalytic system, replacement of the complex CYP and CPR matching system with self-sufficient P450s is an effective strategy to enhance the efficiency of the target product synthesis.

In conclusion, we engineered P450BM3 variants capable of catalyzing C16 $\beta$ , C17 $\alpha$ , C21, and C17 $\alpha$ /21 oxidation of PG and C11 $\alpha$  oxidation of *c* and demonstrated the utility of this transformation in corticosteroids synthesis. In particular, starting from WT-P450BM3, computational simulation-guided substrate channel and heme center remodeling were progressively used for obtaining **VD1721-BM3** to catalyze C17 $\alpha$ /21 oxidation of PG in one step. Our study underscores the immense potential of engineered self-sufficient P450 variants that offer a sustainable, efficient, and versatile pathway for steroids biosynthesis. The integration of advanced computational simulation and synthetic biology presents new opportunities for the synthesis of complex steroid pharmaceuticals.

## ASSOCIATED CONTENT

### Supporting Information

The Supporting Information is available free of charge at <https://pubs.acs.org/doi/10.1021/acscata.3c06137>.

Supporting Information for this work can be found online at the ACS Web site. Materials and methods: chemicals; gene synthesis and plasmid construction; construction of P450BM3 variants library; P450 mutation library screening; P450 variants purification and kinetic parameters analysis; whole-cell catalytic synthesis of 11 $\alpha$ -hydrocortisone and hydrocortisone; molecular docking and molecular dynamics simulation; HPLC, GC-MS, and NMR analysis for the separated and purified products; NMR data; enzyme kinetic parameters analysis of P450s; mechanism analysis for CYP5311B2 and FA11a-BM3 (S7); protein characterization; HPLC analysis for PG hydroxylation; GC-MS analysis for substrates and products; NMR analysis; and MD simulations for P450s and substrate complexes in 100 ns ([PDF](#))

## AUTHOR INFORMATION

### Corresponding Author

Jingwen Zhou – Science Center for Future Foods, School of Biotechnology, Jiangnan University, Wuxi 214122, China; Engineering Research Center of Ministry of Education on Food Synthetic Biotechnology and Jiangsu Province Engineering Research Center of Food Synthetic Biotechnology, Jiangnan University, Wuxi, Jiangsu 214122, China; [orcid.org/0000-0002-3949-3733](https://orcid.org/0000-0002-3949-3733); Email: [zhoujw1982@jiangnan.edu.cn](mailto:zhoujw1982@jiangnan.edu.cn)

### Authors

Ihang Chen – Science Center for Future Foods, School of Biotechnology, Jiangnan University, Wuxi 214122, China; Engineering Research Center of Ministry of Education on Food Synthetic Biotechnology, Jiangnan University, Wuxi, Jiangsu 214122, China

Zikai Chao – Science Center for Future Foods, School of Biotechnology, Jiangnan University, Wuxi 214122, China; Engineering Research Center of Ministry of Education on Food Synthetic Biotechnology, Jiangnan University, Wuxi, Jiangsu 214122, China

Ke Wang – Science Center for Future Foods, School of Biotechnology, Jiangnan University, Wuxi 214122, China; Engineering Research Center of Ministry of Education on

Food Synthetic Biotechnology, Jiangnan University, Wuxi, Jiangsu 214122, China

Xinglong Wang — Science Center for Future Foods, School of Biotechnology, Jiangnan University, Wuxi 214122, China; Engineering Research Center of Ministry of Education on Food Synthetic Biotechnology, Jiangnan University, Wuxi, Jiangsu 214122, China

Hao Meng — Hunan Norchem Pharmaceutical Co., Ltd., Jinshi, Hunan 415400, China

Xirong Liu — Hunan Norchem Pharmaceutical Co., Ltd., Jinshi, Hunan 415400, China

Xiaoyu Shan — Science Center for Future Foods, School of Biotechnology, Jiangnan University, Wuxi 214122, China; Engineering Research Center of Ministry of Education on Food Synthetic Biotechnology, Jiangnan University, Wuxi, Jiangsu 214122, China

Complete contact information is available at:

<https://pubs.acs.org/10.1021/acscatal.3c06137>

## Author Contributions

Q.C., X.S., H.M., X.L., and J.Z. designed the experiments. Q.C. and Z.C performed the molecular biology experiments. Q.C., K.W., and X.W. performed the molecular simulation experiment. Q.C. and J.Z. wrote and revised the manuscript.

## Notes

The authors declare no competing financial interest. This article does not contain any studies with human participants or animals performed by any authors.

## ACKNOWLEDGMENTS

This work has been funded by the National Key Research and Development Program of China (2019YFA0905300).

## REFERENCES

- (1) Zhang, X.; Shen, P.; Zhao, J.; Chen, Y.; Li, X.; Huang, J.-W.; Zhang, L.; Li, Q.; Gao, C.; Xing, Q.; Chen, C.-C.; Guo, R.-T.; Li, A. Rationally Controlling Selective Steroid Hydroxylation via Scaffold Sampling of a P450 Family. *ACS Catal.* **2023**, *13* (2), 1280–1289.
- (2) Simić, S.; Zukić, E.; Schmermund, L.; Faber, K.; Winkler, C. K.; Kroutil, W. Shortening Synthetic Routes to Small Molecule Active Pharmaceutical Ingredients Employing Biocatalytic Methods. *Chem. Rev.* **2022**, *122* (1), 1052–1126.
- (3) Nguyen, K. T.; Virus, C.; Günnewich, N.; Hannemann, F.; Bernhardt, R. Changing the Regioselectivity of a P450 from C15 to C11 Hydroxylation of Progesterone. *ChemBioChem.* **2012**, *13* (8), 1161–1166.
- (4) Chen, W.; Fisher, M. J.; Leung, A.; Cao, Y.; Wong, L. L. Oxidative Diversification of Steroids by Nature-Inspired Scanning Glycine Mutagenesis of P450BM3 (CYP102A1). *ACS Catal.* **2020**, *10* (15), 8334–8343.
- (5) Szczepański, F. M.; Chandelier, C.; Villeret, C.; Masurel, A.; Bourot, S.; Duport, C.; Blanchard, S.; Groisillier, A.; Testet, E.; Costaglioli, P.; Cauet, G.; Degryse, E.; Balbuena, D.; Winter, J.; Achstetter, T.; Spagnoli, R.; Pompon, D.; Dumas, B. Total biosynthesis of hydrocortisone from a simple carbon source in yeast. *Nat. Biotechnol.* **2003**, *21* (2), 143–149.
- (6) Li, F.; Deng, H.; Renata, H. Remote B-Ring Oxidation of Sclareol with an Engineered P450 Facilitates Divergent Access to Complex Terpenoids. *J. Am. Chem. Soc.* **2022**, *144* (17), 7616–7621.
- (7) Rizzuto, F. J.; Carpenter, J. P.; Nitschke, J. R. Multisite Binding of Drugs and Natural Products in an Entropically Favorable, Heteroleptic Receptor. *J. Am. Chem. Soc.* **2019**, *141* (22), 9087–9095.
- (8) Peng, Y.; Gao, C.; Zhang, Z.; Wu, S.; Zhao, J.; Li, A. A Chemoenzymatic Strategy for the Synthesis of Steroid Drugs Enabled by P450 Monooxygenase-Mediated Steroidal Core Modification. *ACS Catal.* **2022**, *12* (5), 2907–2914.
- (9) Emmanuel, M. A.; Bender, S. G.; Bilodeau, C.; Carceller, J. M.; DeHovitz, J. S.; Fu, H.; Liu, Y.; Nicholls, B. T.; Ouyang, Y.; Page, C. G.; Qiao, T.; Raps, F. C.; Sorigué, D. R.; Sun, S.-Z.; Turek-Herman, J.; Ye, Y.; Rivas-Souchet, A.; Cao, J.; Hyster, T. K. Photobiocatalytic Strategies for Organic Synthesis. *Chem. Rev.* **2023**, *123* (9), 5459–5520.
- (10) Stout, C. N.; Wasfy, N. M.; Chen, F.; Renata, H. Charting the Evolution of Chemoenzymatic Strategies in the Syntheses of Complex Natural Products. *J. Am. Chem. Soc.* **2023**, *145* (33), 18161–18181.
- (11) Acevedo-Rocha, C. G.; Gamble, C. G.; Lonsdale, R.; Li, A.; Nett, N.; Hoebenreich, S.; Lingnau, J. B.; Wirtz, C.; Fares, C.; Hinrichs, H.; Dege, A.; Mulholland, A. J.; Nov, Y.; Leys, D.; McLean, K. J.; Munro, A. W.; Reetz, M. T. P450-Catalyzed Regio- and Diastereoselective Steroid Hydroxylation: Efficient Directed Evolution Enabled by Mutability Landscaping. *ACS Catal.* **2018**, *8* (4), 3395–3410.
- (12) Bellotti, P.; Huang, H.-M.; Faber, T.; Glorius, F. Photocatalytic Late-Stage C–H Functionalization. *Chem. Rev.* **2023**, *123* (8), 4237–4352.
- (13) Kim, H.; Rogler, P. J.; Sharma, S. K.; Schaefer, A. W.; Solomon, E. I.; Karlin, K. D. Heme-FeIII Superoxide, Peroxide and Hydroperoxide Thermodynamic Relationships: FeIII-O<sub>2</sub>•– Complex H-Atom Abstraction Reactivity. *J. Am. Chem. Soc.* **2020**, *142* (6), 3104–3116.
- (14) Li, Z.; Meng, S.; Nie, K.; Schwaneberg, U.; Davari, M. D.; Xu, H.; Ji, Y.; Liu, L. Flexibility Regulation of Loops Surrounding the Tunnel Entrance in Cytochrome P450 Enhanced Substrate Access Substantially. *ACS Catal.* **2022**, *12* (20), 12800–12808.
- (15) Chen, J.; Fan, F.; Qu, G.; Tang, J.; Xi, Y.; Bi, C.; Sun, Z.; Zhang, X. Identification of *Absidia orchidis* steroid 11β-hydroxylation system and its application in engineering *Saccharomyces cerevisiae* for one-step biotransformation to produce hydrocortisone. *Metab Eng.* **2020**, *57*, 31–42.
- (16) Zollner, A.; Kagawa, N.; Waterman, M. R.; Nonaka, Y.; Takio, K.; Shiro, Y.; Hannemann, F.; Bernhardt, R. Purification and functional characterization of human 11beta hydroxylase expressed in *Escherichia coli*. *FEBS J.* **2008**, *275* (4), 799–810.
- (17) Schiffer, L.; Anderko, S.; Hobler, A.; Hannemann, F.; Kagawa, N.; Bernhardt, R. A recombinant CYP11B1 dependent *Escherichia coli* biocatalyst for selective cortisol production and optimization towards a preparative scale. *Microb. Cell Fact* **2015**, *14* (1), 25.
- (18) Carroll, E.; Ravi Gopal, B.; Raghavan, I.; Mukherjee, M.; Wang, Z. Q. A cytochrome P450 CYP87A4 imparts sterol side-chain cleavage in digoxin biosynthesis. *Nat. Commun.* **2023**, *14* (1), 4042.
- (19) Zhang, R.; Zhang, Y.; Wang, Y.; Yao, M.; Zhang, J.; Liu, H.; Zhou, X.; Xiao, W.; Yuan, Y. Pregnenolone Overproduction in *Yarrowia lipolytica* by Integrative Components Pairing of the Cytochrome P450scc System. *ACS Synth. Biol.* **2019**, *8* (12), 2666–2678.
- (20) Chen, Q. H.; Qian, Y. D.; Niu, Y. J.; Hu, C. Y.; Meng, Y. H. Characterization of an efficient CRISPR-iCas9 system in *Yarrowia lipolytica* for the biosynthesis of carotenoids. *Appl. Microbiol. Biotechnol.* **2023**, *107* (20), 6299–6313.
- (21) Clark, B. J.; Waterman, M. R. The hydrophobic amino-terminal sequence of bovine 17 alpha-hydroxylase is required for the expression of a functional hemoprotein in COS 1 cells. *J. Biol. Chem.* **1991**, *266* (9), 5898–5904.
- (22) Grischuk, Y.; Rubtsov, P.; Riepe, F. G.; Grötzinger, J.; Beljarskaia, S.; Prassolov, V.; Kalintchenko, N.; Semitcheva, T.; Peterkova, V.; Tiulpakov, A.; Sippell, W. G.; Krone, N. Four Novel Missense Mutations in the CYP21A2 Gene Detected in Russian Patients Suffering from the Classical Form of Congenital Adrenal Hyperplasia: Identification, Functional Characterization, and Structural Analysis. *J. Clin Endocr Metab* **2006**, *91* (12), 4976–4980.
- (23) Pallan, P. S.; Wang, C.; Lei, L.; Yoshimoto, F. K.; Auchus, R. J.; Waterman, M. R.; Guengerich, F. P.; Egli, M. Human Cytochrome P450 21A2, the Major Steroid 21-Hydroxylase: Structure of the

- enzyme·progesterone substrate complex and rate-limiting C-H bond cleavage. *J. Biol. Chem.* **2015**, *290* (21), 13128–43.
- (24) Pan, H.; Chang, S.; Qu, Y.; Liu, M.; Tian, W.; Chang, Z. Hydrocortisone production using whole-cell biocatalysts in recombinant *Escherichia coli*. *Biochem Eng. J.* **2023**, *198*, No. 109023, DOI: 10.1016/j.bej.2023.109023.
- (25) Kille, S.; Zilly, F. E.; Acevedo, J. P.; Reetz, M. T. Regio- and stereoselectivity of P450-catalysed hydroxylation of steroids controlled by laboratory evolution. *Nat. Chem.* **2011**, *3* (9), 738–743.
- (26) Guengerich, F. P. Mechanisms of Cytochrome P450-Catalyzed Oxidations. *ACS Catal.* **2018**, *8* (12), 10964–10976.
- (27) Wu, Z.-M.; Xie, F.; Zheng, W.; Liu, C.-F.; Lin, C.-P.; Zheng, R.-C.; Zheng, Y.-G. Structure-Oriented Engineering of Amidase: Modification of Twisted Access Tunnel for Efficient Synthesis of 2-Chloronicotinic Acid. *ACS Catal.* **2023**, *13* (13), 9078–9089.
- (28) Li, R.-J.; Tian, K.; Li, X.; Gaikaiwari, A. R.; Li, Z. Engineering P450 Monooxygenases for Highly Regioselective and Active p-Hydroxylation of m-Alkylphenols. *ACS Catal.* **2022**, *12* (10), 5939–5948.
- (29) Acevedo-Rocha, C. G.; Li, A.; D'Amore, L.; Hoebenreich, S.; Sanchis, J.; Lubrano, P.; Ferla, M. P.; Garcia-Borràs, M.; Osuna, S.; Reetz, M. T. Pervasive cooperative mutational effects on multiple catalytic enzyme traits emerge via long-range conformational dynamics. *Nat. Commun.* **2021**, *12* (1), 1621.
- (30) Brezovsky, J.; Babkova, P.; Degtarik, O.; Fortova, A.; Gora, A.; Iermak, I.; Rezavova, P.; Dvorak, P.; Smatanova, I. K.; Prokop, Z.; Chaloupkova, R.; Damborsky, J. Engineering a de Novo Transport Tunnel. *ACS Catal.* **2016**, *6* (11), 7597–7610.
- (31) Kouba, P.; Kohout, P.; Haddadi, F.; Bushuiev, A.; Samusevich, R.; Sedlar, J.; Damborsky, J.; Pluskal, T.; Sivic, J.; Mazurenko, S. Machine Learning-Guided Protein Engineering. *ACS Catal.* **2023**, *13* (21), 13863–13895.
- (32) Chen, Q. H.; Xie, D. T.; Qiang, S.; Hu, C. Y.; Meng, Y. H. Developing efficient vanillin biosynthesis system by regulating feruloyl-CoA synthetase and enoyl-CoA hydratase enzymes. *Appl. Microbiol. Biotechnol.* **2022**, *106* (1), 247–259.
- (33) Kille, S.; Zilly, F. E.; Acevedo, J. P.; Reetz, M. T. Regio- and stereoselectivity of P450-catalysed hydroxylation of steroids controlled by laboratory evolution. *Nat. Chem.* **2011**, *3* (9), 738–43.
- (34) Sun, Z.; Liu, Q.; Qu, G.; Feng, Y.; Reetz, M. T. Utility of B-Factors in Protein Science: Interpreting Rigidity, Flexibility, and Internal Motion and Engineering Thermostability. *Chem. Rev.* **2019**, *119* (3), 1626–1665.
- (35) Zhang, Z.; Gao, C.; Zhao, J.; Peng, X.-G.; Li, Q.; Li, A. A Designed Chemoenzymatic Route for Efficient Synthesis of 6-Dehydronandrolone Acetate: A Key Precursor in the Synthesis of C7-Functionalized Steroidal Drugs. *ACS Catal.* **2023**, *13* (19), 13111–13116.
- (36) Miller, J. C.; Lee, J. H. Z.; McLean, M. A.; Chao, R. R.; Stone, I. S. J.; Pukala, T. L.; Brunning, J. B.; De Voss, J. J.; Schuler, M. A.; Sligar, S. G.; Bell, S. G. Engineering C-C Bond Cleavage Activity into a P450 Monooxygenase Enzyme. *J. Am. Chem. Soc.* **2023**, *145* (16), 9207–9222.
- (37) Valdés-Tresanco, M. S.; Valdés-Tresanco, M. E.; Valiente, P. A.; Moreno, E. gmx\_MMPBSA: A New Tool to Perform End-State Free Energy Calculations with GROMACS. *J. Chem. Theory Comput.* **2021**, *17* (10), 6281–6291.
- (38) Li, A.; Acevedo-Rocha, C. G.; D'Amore, L.; Chen, J.; Peng, Y.; Garcia-Borràs, M.; Gao, C.; Zhu, J.; Rickerby, H.; Osuna, S.; Zhou, J.; Reetz, M. T. Regio- and Stereoselective Steroid Hydroxylation at C7 by Cytochrome P450 Monooxygenase Mutants. *Angew. Chem., Int. Ed. Engl.* **2020**, *59* (30), 12499–12505.
- (39) Marshall, L. R.; Bhattacharya, S.; Korendovych, I. V. Fishing for Catalysis: Experimental Approaches to Narrowing Search Space in Directed Evolution of Enzymes. *JACS Au* **2023**, *3* (9), 2402–2412.
- (40) Chen, Q.; Jiang, Y.; Kang, Z.; Cheng, J.; Xiong, X.; Hu, C. Y.; Meng, Y. Engineering a feruloyl-coenzyme a synthase for bioconversion of phenylpropanoid acids into high-value aromatic aldehydes. *J. Agric. Food Chem.* **2022**, *70* (32), 9948–9960.
- (41) Rapp, L. R.; Marques, S. M.; Zukic, E.; Rowlinson, B.; Sharma, M.; Grogan, G.; Damborsky, J.; Hauer, B. Substrate Anchoring and Flexibility Reduction in CYP153AM.aq Leads to Highly Improved Efficiency toward Octanoic Acid. *ACS Catal.* **2021**, *11* (5), 3182–3189.
- (42) Sánchez-Morán, H.; Gonçalves, L. R. B.; Schwartz, D. K.; Kaar, J. L. Framework for Optimizing Polymeric Supports for Immobilized Biocatalysts by Computational Analysis of Enzyme Surface Hydrophobicity. *ACS Catal.* **2023**, *13* (7), 4304–4315.
- (43) Zhang, L.; Xie, Z.; Liu, Z.; Zhou, S.; Ma, L.; Liu, W.; Huang, J. W.; Ko, T. P.; Li, X.; Hu, Y.; Min, J.; Yu, X.; Guo, R. T.; Chen, C. C. Structural insight into the electron transfer pathway of a self-sufficient P450 monooxygenase. *Nat. Commun.* **2020**, *11* (1), 2676.
- (44) Yang, J.; Liu, Y.; Zhong, D.; Xu, L.; Gao, H.; Keasling, J. D.; Luo, X.; Chou, H. H. Combinatorial optimization and spatial remodeling of CYPs to control product profile. *Metab Eng.* **2023**, *80*, 119–129.